"Dipolar filming" of protein motion using electron paramagnetic resonance (EPR); Development of anti-reflective coating (ARC) for subterahertz lens

Johanna Schubert
2022 Physics REU, Department of Physics, University of California, Santa Barbara and Department of Physics, Swarthmore College

Brad Price (Graduate Advisor) and Mark Sherwin (Faculty Advisor)
Department of Driven and Quantum Biological Matter, University of California, Santa Barbara
(Dated: September 24, 2022)

I. Explaining protein function relies on understanding protein motion in response to external stimuli. We combine electron paramagnetic resonance (EPR) spectroscopy at high magnetic fields (8.62T, 240 GHz) with site-directed spin-labeling to study the structural dynamics of AsLOV2, a blue-light activated phototropin. In this experiment, AsLOV2 samples with a glutamine-to-alanine point mutation at site 513 were activated by a 450 nm laser prior to measuring absorbance over time. Relaxation times for UV-Vis and time-swept EPR data were found to be 135.2±0.6 s and 102.8±0.5 s, respectively, for AsLOV2 Q513A mutant, suggesting that the protein regains its ordered structure before its light-absorbing chromophore has recovered. II. Sherwin Lab conducts high-power, pulsed EPR at high magnetic fields by generating two pulses from the UCSB free-electron laser (FEL) with the use of pulse slicing quasioptics. However, backscattering at the quasioptics introduces standing waves and causes a spectrometer dead time of 70 ns. 3D-printing an anti-reflective coating for the EPR lens was the second half of my project. We used effective medium approximations (Bruggeman's model) by manipulating the infill density of solid polylactic acid slabs to achieve the desired effective refractive index. This involved designing a repetitive "step" infill to print thin solid slabs with varying density.

EPR FOR PROTEIN DYNAMICS

I. INTRODUCTION

Proteins are nano-sized dynamic molecules that enable life. Many protein structures are readily mapped in three-dimensions using methods such as x-ray crystallography, (solid-state) nuclear magnetic resonance imaging (NMR), and more recently cryo electron microscopy [1]. The protein data bank (PDB) currently contains over 190,000 3D protein structures [2]. While protein structure is well-understood, explaining protein function requires understanding how proteins move when activated by physical and chemical stimuli [3]. We combine high-field (8.62T, 240 GHz) electron paramagnetic resonance (EPR) spectroscopy with site-directed spin-labelling (SDSL) to study the reversible dynamics of AsLOV2, a blue-light activated phototropin derived from oats (Figure 1). In this experiment, we study the dynamics of the AsLOV2 Q513A mutant, which contains a glutamine-to-alanine point mutation at site 513 [4]. Comparing UV-Visible light and EPR transients enables us to make a connection between light absorption and protein motion.

FIG. 1. Unactivated dark state of light-adapted wild-type AsLOV2 mapped using x-ray crystallography [5].

II. THEORY

A. Electron Paramagnetic Resonance Spectroscopy

Electron paramagnetic resonance (EPR) spectroscopy exploits the quantum mechanical properties of materials that contain unpaired electrons. For field-swept EPR measurements, the magnetic field B_0 is swept near a resonant magnetic field value B_{res} that depends on a chosen frequency ω which is held constant. In the simplest case, electron ($|m_s| = 1/2$) spins are either spin-up ($m_s = +1/2$) or spin-down ($m_s = -1/2$) according to Quantum Mechanics. Due to the Maxwell-Boltzmann distribution, slightly more spins are spin-up near B_{res}. Hence, sweeping the field near B_{res} causes more transitions from spin-down to spin-up than the reverse, which yields a net absorption of energy $\triangle E$ which is measured and recorded in a spectrum (Figure 2). The governing equation for EPR spectroscopy follows:

$$\triangle E = \hbar\omega = g_e \mu_B B_0 \quad (1)$$

where $\hbar$ is reduced Planck's constant, ω is the chosen frequency, g_e is the electron spin g factor, μ_B is the Bohr magnetron, and B_0 is the applied magnetic field [6].

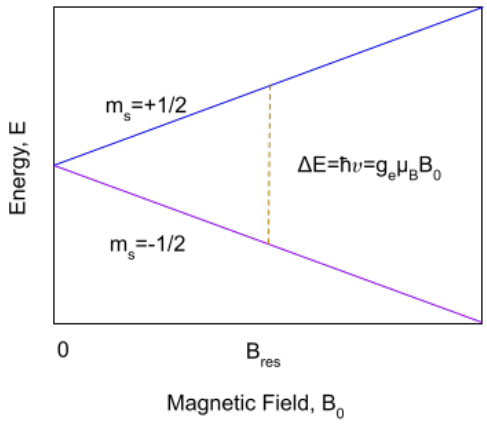

FIG. 2. Energy spectrum of spin-1/2 particles in a magnetic field.

B. Protein Tumbling in Solution

The effective spin Hamiltonian of the spin labels contains a dipolar coupling given by

$$H_{dd} = \omega_{dd}^0 (S_z^A S_z^B - \tfrac{1}{4}(S_+^A S_-^B + S_-^A S_+^B))(3cos^2\theta_d - 1). \quad (2)$$

where ω_{dd}^0 is the coupling constant, S_z^A and S_z^B are the spins on the protein labels, and θ_d is the angle between the spin labels [7]. Due to the effects of tumbling, θ_d changes constantly and randomly (see figure 3). According to the ergodic hypothesis, all microstates of a system are accessed over sufficiently long time scales. This is potentially problematic, as the time-average of the dipolar coupling term goes to zero over long time scales, and our type of EPR depends on this term. Although we are able to observe differences in EPR lineshape for AsLOV2 in its ordered and activated state without accounting for the effects of tumbling, we do not have a good estimate about our proximity to the static limit [8].

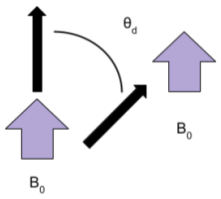

FIG. 3. Angle between spin labels in a static magnetic field.

III. METHODS

The blue light (450 nm) chromophore activation of AsLOV2 Q513A was quantified by measuring the transmission of 447 nm light passed through the protein sample. UV-Visible light spectroscopy was used to determine the transient after a short (approx. 30 s) blue light exposure (Figure 4). Field-swept cwEPR (8.62 T, 240 GHz) measurements were performed with and without blue light activation at 450 nm. The transient of cwEPR was measured at the field of maximum amplitude after a short (5 s) sample blue light exposure. The 447-nm-transmission and cwEPR transients were compared by writing Python code to fit a decaying exponential to the average of the two scans performed for each. The fitting function used was

$$s(t) = a + be^{-t/\tau}, \quad (4)$$

where t is time, $s(t)$ is the transient, a and b are arbitrary constants, and τ is the relaxation time. The error in the relaxation time τ was found from the covariance matrix by taking two times the square root of the covariance for τ, which gives a 95% confidence for the extracted τ value.

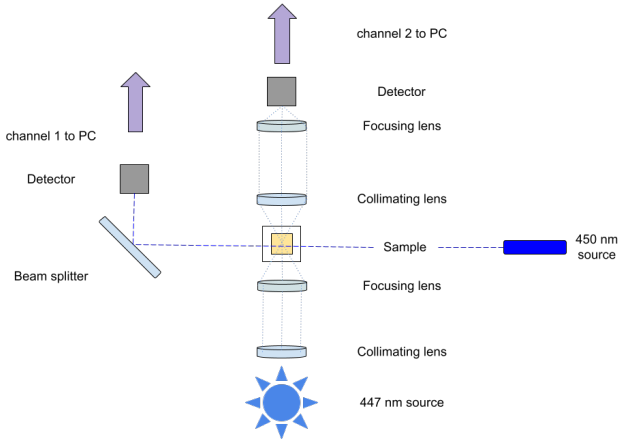

FIG. 4. Triggered UV-Visible spectroscopy set-up.

IV. RESULTS

The maximum amplitude for 450 nm activated cwEPR was at B_0+4.62 mT (Figure 5). cwEPR amplitude versus time data at $B_0 + 4.62$ mT yielded a relaxation time of $\tau = 102.8 \pm 0.5$ s (Figure 6a). In comparison, transient transmitted intensity of 447 nm under 450 nm activation yielded a relaxation time $\tau = 135.2 \pm 0.6$ s (Figure 6b).

V. DISCUSSION

The discrepancy between the relaxation times for the 447-nm-transmission and cwEPR transients suggests that the 3D-protein structure returns to its unactivated

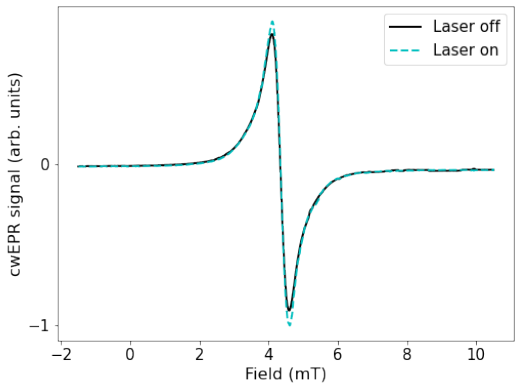

FIG. 5. Field-swept EPR spectrum of AsLOV2 Q513A mutant highlighting spectroscopic changes upon 450 nm blue-light activation. Solid black line is laser off and dashed blue line is laser on.

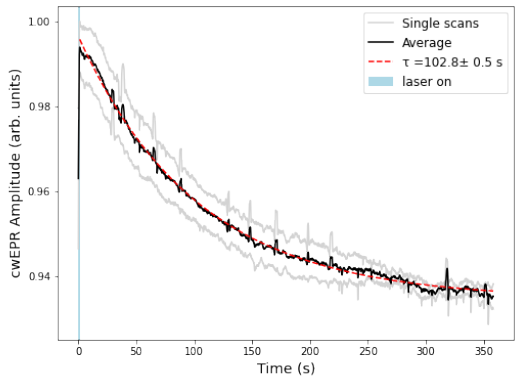

FIG. 6. cwEPR amplitude vs. time at $B_0 + 4.62$ mT for asLOV2 Q513A mutant, the blue-light laser on time is 5 s, the timestep is $\triangle t = 60$ ms, the relaxation time constant is $\tau = 102.8 \pm 0.5$ s.

configuration before the chromophore completely releases all absorbed light. Relaxation times are approximately half as long for wild type AsLOV2, which were previously measured to be 65 s and 52 s for the 447-nm-transmission and cwEPR transients respectively [3]. This slowdown in relaxation times is expected because the Q513A mutation disrupts hydrogen bonding that aids the folding process of one of the helices [9].

VI. FURTHER WORK

Determining the extent to which the tumbling of AsLOV2 samples suspended in solution is affecting cwEPR measurements remains an important task. One option is to try using different gelling agents to physically inhibit protein motion, and to see if there are any

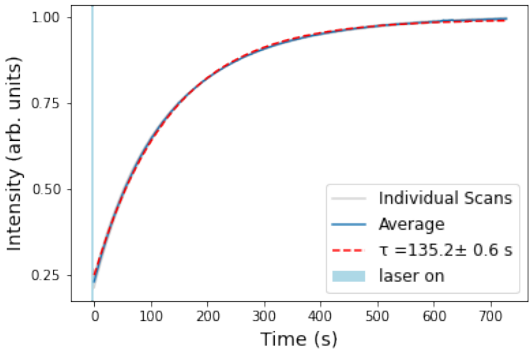

FIG. 7. 447 nm transmitted intensity vs. time for AsLOV2 Q513A mutant, the time step is $\triangle = 1$ s, the relaxation time constant is $\tau = 135.2 \pm 0.6$ s.

changes in the field-swept cwEPR lineshape. Another option would be to quantify the rotational correlation time of AsLOV2 suspended in solution. The rotational correlation time can be estimated from the $T_1 : T_2$ relaxation ratio, where T_1 is the longitudinal magnetization recovery and T_2 is the transverse magnetization decay. T_1 and T_2 measurements can be performed at room-temperature using NMR [10].

ARC FOR PULSED EPR LENS

VII. INTRODUCTION

The terahertz range lies at the far end of the infrared region before the microwave region and is difficult to access because viable sources and detectors are expensive [11]. For performing EPR measurements, higher applied magnetic fields are desirable but require high power sources. Sherwin Lab uses quasioptics to generate pulses from the UCSB free-electron laser which drive high-power, pulsed EPR at high fields. In the current set-up, backscattering from the three lenses introduces signal interference and causes a spectrometer dead time of approximately 70 ns [12]. A second task for the project was to develop a 3D-printed anti-reflective coating (ARC) to eliminate retroflected electromagnetic waves and reduce dead time.

VIII. THEORY

A. Anti-Reflective Optics

The optics for the anti-reflective coating (ARC) are shown in Figure 8. We can tune the optical thickness of the ARC to be an integer multiple of $\lambda/4$ so that waves that reflect from the air-ARC and the ARC-lens interphases have a π phase shift and therefore interfere

deconstructively. For an assymetric Fabry-Perot cavity, i.e. ambient (n_{air}), ARC of thickness d (n_{ARC}), and lens (n_{HDPE}), the conditions for the maximum percent of transmitted light occur when $n_{ARC} = \sqrt{n_{air} n_{HDPE}}$ [13].

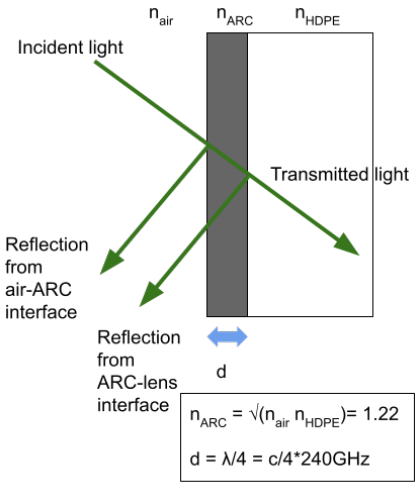

FIG. 8. Schematic of anti-reflective optics.

B. Effective Medium Approximations

It is difficult to find materials that have a lower refractive index than high-density polyethylene (HDPE), the material used in the EPR lenses. Therefore, using an effective medium is the only reasonable solution. Bruggeman's model relates fill fraction (f), the dielectric function of the 100% infill material ($\epsilon = n^2$), and the dielectric function of the composite structure ($\epsilon_{eff} = n_{eff}^2$). Using the assumption that absorption is negligible for a thin enough plate, we use Bruggeman's model in the form:

$$\frac{3f}{2+\frac{n^2}{n_{eff}^2}} + \frac{3(1-f)}{2+\frac{1}{n_{eff}^2}} = 1 \ (6). \ [14]$$

IX. METHODS

A vector network analyzer (VNA) was used to take phase measurements. A small frequency region was isolated around 240 GHz with a span of 26 MHz as this is the mode spacing on the free electron laser (FEL). The equation used to find n follows:

$$n = \frac{c\theta}{2\pi d \cdot \omega} + n_{air} \ (7)$$

where c is the speed of light, θ is the phase difference, d is the thickness and ω is the frequency [15].

Infill patterns in 3D printer slicing software are typically used to change the infill density of 3D-printed solid structures. However, these patterns are usually crosshatch patterns that leave gaps in the overall structure. Hence, we designed the PLA slabs to have the desired density in the 3D printing design software and printed at 100% infill density (Figure 9).

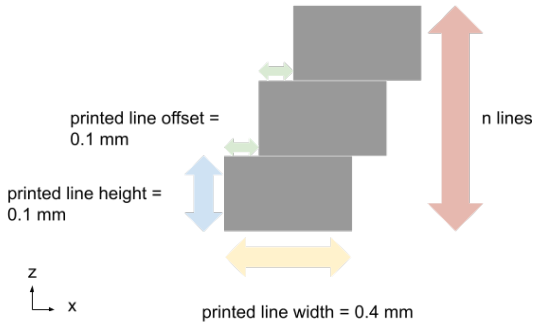

FIG. 9. Side view of infill design structure. The number of layers n determines the thickness. The PLA slab is constructed by repeating the infill structure in the x-direction and extruding each structure in the y-direction. Infill density is manipulated by varying the distance between each repeating infill structure.

X. RESULTS

VNA phase difference versus frequency measurements for 100% and 52.5% infill PLA slabs with thicknesses $d = 0.560 \pm 0.005$ cm and $d = 1.500 \pm 0.005$ cm, respectively, are shown in Figure 10. The refractive index n for the 100% infill slab was found to be 1.44 ± 0.01, which is within 1% of the expected value for PLA, suggesting small systematic error. Applying Bruggeman's model with $n_{measured} = 1.44$ and $n_{effective} = 1.22$ yields a percent infill $\rho = 52.5\%$. The measured refractive index n of the 52.5% infill PLA slab was found to be $n_{measured} = 1.28 \pm 0.01$, which is within 5% of n_{eff}, suggesting small systematic error assuming that Bruggeman's model is valid. The RMS deviation of the phase difference from the average phase difference in the region used to calculate n was negligible. Hence, the error in the refractive index measurement is carried over from the error in the thickness d.

XI. DISCUSSION AND FUTURE WORK

The percent infill must be optimized to achieve $n_{eff} = 1.22$ by testing several values of f near 52.5%. Figures 12 and 13 show periodic wiggles in phase versus frequency data. We hypothesize the infill design creates a partial polarizer. The polarization properties of the PLA slabs can be tested by performing phase difference measurements as a function of rotation. Ultimately, we want an isotropic infill pattern. The final ARC must be printed

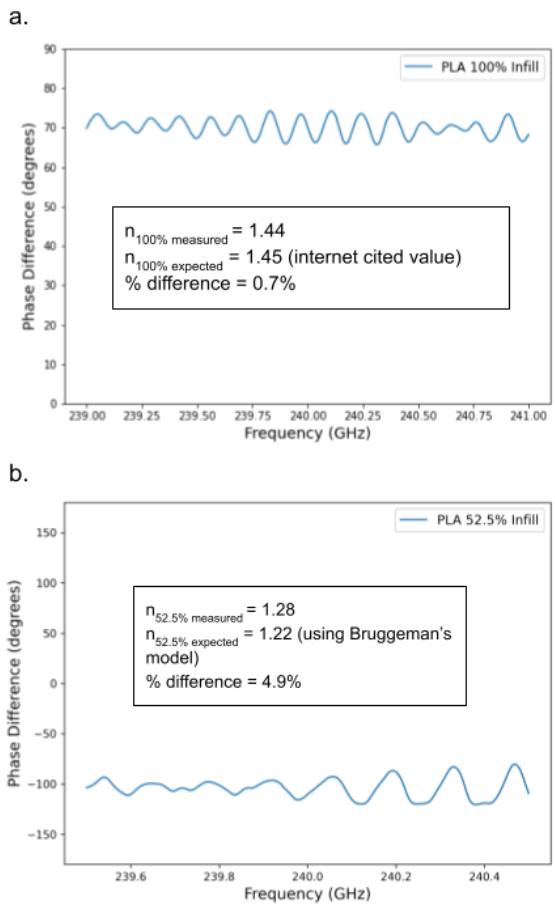

FIG. 10. Phase difference versus frequency and refractive index measurement of a) 100% and b) 52.5% infill PLA slabs.

with the correct dimensions for mounting onto the backside of the EPR lens, which has minimal curvature.

ACKNOWLEDGMENTS

I would like to thank Brad Price for his support and mentorship, and Dr. Mark Sherwin for enabling me to pursue my interests and perform research I am excited about. Thank you also to Dr. Sathya Guruswamy for giving me the incredible opportunity to participate in the UCSB Physics REU program, and to NSF REU grant PHY-1852574 for funding this experience. I would also like to thank the Sherwin Lab group and my REU cohort for providing a welcoming and engaging environment for professional and personal growth. Lastly, I would like to thank the Swarthmore Physics department.

[1] J. W. Taraska, enMapping membrane protein structure with fluorescence, Current Opinion in Structural Biology Engineering and design / Membranes, **22**, 507 (2012).
[2] PDB, Protein Data Bank, `https://www.rcsb.org/`.
[3] B. Price", S. Maity, Triggered functional dynamics of aslov2 by time-resolved electron paramagnetic resonance at high magnetic fields, In submission (2022).
[4] J. Dietler, R. Gelfert, J. Kaiser, V. Borin, C. Renzl, S. Pilsl, A. T. Ranzani, A. García de Fuentes, T. Gleichmann, R. P. Diensthuber, M. Weyand, G. Mayer, I. Schapiro, and A. Möglich, enSignal transduction in light-oxygen-voltage receptors lacking the active-site glutamine, Nature Communications **13**, 2618 (2022).
[5] PyMOL, `https://pymol.org/2/`.
[6] E. Duin, Electron paramagnetic resonance theory, (2013).
[7] M. H. Levitt, Spin dynamics: Basics of nuclear magnetic resonance chapter 19, (2008).
[8] B. Price, Triggered functional dynamics of aslov2 by time-resolved electron paramagnetic resonance at high magnetic fields (advancement to candidacy) (2022).
[9] P. L. Freddolino, K. H. Gardner, and K. Schulten, enSignaling mechanisms of LOV domains: new insights from molecular dynamics studies, Photochemical & Photobiological Sciences **12**, 1158 (2013), publisher: The Royal Society of Chemistry.
[10] D. Dai, Room-temperature dynamic nuclear polarization enhanced nmr spectroscopy of small biological molecules in water, (2021).
[11] B. D. Price, S. N. Lowry, I. D. Hartley, and M. Reid, Subterahertz refractive flat-top beam shaping via 3d printed aspheric lens combination, Appl. Opt. **59**, 5429 (2020).
[12] S. Takahashi, Free-electron laser-powered electron paramagnetic resonance spectroscopy, Nature (2012).
[13] J. Krepelka, Maximally flat antireflection coatings, Jemná Mechanika A Optika **3**, 53 (1992).
[14] N. Agladze, Laboratory results on millimeter-wave absorption in silicate grain materials at cryogenic temperatures., The Astrophysical Journal (1996).
[15] C. B. Wilson, S. Aronson, J. A. Clayton, S. J. Glaser, S. Han, and M. S. Sherwin, Multi-step phase-cycling in a free-electron laser-powered pulsed electron paramagnetic resonance spectrometer, Phys. Chem. Chem. Phys. **20**, 18097 (2018).